

Yigit S, Chakraborty N.

[Influences of aspect ratio on natural convection of power-law fluids in cylindrical annular space with differentially heated vertical walls.](#)

Thermal Science and Engineering Progress 2017, 2, 151-164.

Copyright:

© 2017. This manuscript version is made available under the [CC-BY-NC-ND 4.0 license](#)

DOI link to article:

<https://doi.org/10.1016/j.tsep.2017.05.008>

Date deposited:

18/05/2017

Embargo release date:

21 May 2019




This work is licensed under a [Creative Commons Attribution-NonCommercial-NoDerivatives 4.0 International licence](#)

Influences of aspect ratio on natural convection of power-law fluids in cylindrical annular space with differentially heated vertical walls

Sahin Yigit¹, and Nilanjan Chakraborty ¹

¹School of Mechanical and Systems Engineering, Newcastle University, Newcastle-Upon-Tyne, NE1 7RU, UK

 Corresponding author.

s.yigit1@ncl.ac.uk

KEYWORDS: Natural convection, non-Newtonian fluids, Power-law model, cylindrical annular enclosure, aspect ratio.

ABSTRACT

Natural convection of power-law fluids in cylindrical annular spaces has not been analysed in detail in spite of its industrial importance in food and chemical processing, solar collectors, cooling of electronics. Therefore, laminar natural convection of power-law fluids in rectangular cross-sectional cylindrical annular spaces with differentially heated vertical walls subjected to the both constant wall temperature (CWT), and constant wall heat flux (CWHF) boundary conditions has been investigated in this study. Two-dimensional axisymmetric steady-state numerical simulations have been conducted for a range of values of normalized internal radius $0.125 \leq r_i/L \leq 16$ (where r_i internal cylinder radius, L is the difference between outer and inner cylinder radius), aspect ratio $0.125 \leq AR \leq 8$ ($AR = H/L$, where H is the enclosure height), power-law index (i.e. $0.6 \leq n \leq 1.8$) and nominal Rayleigh number (i.e. $Ra = 10^3 - 10^6$) for a single value of nominal Prandtl number: $Pr = 10^3$. It is found that the mean Nusselt number based on the inner periphery of the annular space \overline{Nu}_i increases with an increase in Ra due to the strengthening of buoyancy forces. By contrast, \overline{Nu}_i increases with a decrease in n due to the weakening of viscous resistance. The mean Nusselt number \overline{Nu}_i decreases with an increase in r_i/L before approaching the mean Nusselt number for a rectangular enclosure in the limit of $r_i/L \rightarrow \infty$. By contrast \overline{Nu}_i normalized by the corresponding Nusselt number for pure conduction (i.e. $\overline{Nu}_i/Nu_{cond}$) increases with an increase in r_i/L . The contribution of convection to overall thermal transport strength increases with an increase in r_i/L , since the Nusselt number for pure conductive transport Nu_{cond} decreases with an increase in r_i/L for cylindrical annular spaces. Additionally, it has been found that \overline{Nu}_i exhibits a non-monotonic variation with an increase in AR for same set of values of $Ra, Pr, r_i/L$ for shear thinning ($n < 1$), Newtonian ($n = 1$) and shear thickening ($n > 1$) fluids in the CWT configuration, while \overline{Nu}_i increases monotonically with an increase in AR in the CWHF configuration irrespective of the value of n . The completion between the strengthening of thermal convection and the weakening of conductive thermal transport with an increase in AR is responsible for the non-monotonic AR dependence of \overline{Nu}_i in the CWT boundary condition. A scaling analysis is utilized to explain the influences of normalized radius, aspect ratio, nominal Rayleigh and Prandtl numbers, power-law index on \overline{Nu}_i for natural convection of power-law fluids within rectangular cross-sectional cylindrical annular spaces. Finally, new correlations have been proposed for \overline{Nu}_i for both CWT and CWHF boundary conditions, which have been shown to provide satisfactorily predictions of \overline{Nu}_i for the range of the parameters considered in this analysis.

NOMENCLATURE

AR	[-]	Aspect ratio ($AR=H/L$)
b, b_2	[-]	Correlation parameter
c_2, c_3	[-]	Correlation parameters
c_p	[J/kgK]	Specific heat at constant pressure
d	[-]	Correlation parameter
e	[-]	Relative error
e_{ij}	[s ⁻¹]	Rate of strain tensor
g	[m/s ²]	Gravitational acceleration
Gr	[-]	Grashof number
H	[-]	Height of cylindrical enclosure
h	[W/m ² K]	Heat transfer coefficient
K	[N.s ⁿ /m ²]	Consistency
k	[W/mK]	Thermal conductivity
L	[m]	Difference between outer and inner cylinder radius
m	[-]	Correlation parameter
n	[-]	Power-law index
\overline{Nu}	[-]	Mean Nusselt number
\overline{Nu}_i	[-]	Mean Nusselt number on the inner periphery
P	[Pa]	Pressure
Pr	[-]	Prandtl number
q	[W/m ²]	Heat flux
r	[m]	Radius
r_i	[m]	Inner radius
r_o	[m]	Outer radius

Ra	[-]	Rayleigh number
T	[K]	Temperature
u_i	[m/s]	i^{th} velocity component
U, W	[-]	Dimensionless radial ($U = u_r L / \alpha$) and vertical velocity ($W = u_3 L / \alpha$)
U_{ref}	[m/s]	Reference velocity scale
\mathcal{G}	[m/s]	Characteristic velocity
x_i	[m]	Coordinate in i^{th} direction
α	[m ² /s]	Thermal diffusivity
β	[1/K]	Coefficient of thermal expansion
δ, δ_{th}	[m]	Velocity and thermal boundary-layer thickness
θ	[-]	Dimensionless temperature
μ	[Ns/m ²]	Dynamic viscosity
ν	[m ² /s]	Kinematic viscosity
ρ	[kg/m ³]	Density
$\tau_{ij} (\tau)$	[Pa]	Stress tensor (stress)
ϕ	[-]	Azimuthal co-ordinate
Ψ	[-]	Dimensionless stream function

Subscripts

a	Apparent
C	Cold wall
CWT	Constant wall temperature
$CWHF$	Constant wall heat flux
$cond$	Conduction
eff	Effective value
ext	Extrapolated value

<i>H</i>	Hot wall
<i>i</i>	Inner periphery
<i>max</i>	Maximum value
<i>min</i>	Minimum value
<i>nom</i>	Nominal value
<i>o</i>	Outer periphery
<i>ref</i>	Reference value
<i>rec</i>	Rectangular
<i>wall</i>	Wall value
<i>wi</i>	Inner periphery wall
<i>wo</i>	Outer periphery wall

Special characters

ΔT	[K]	Difference between hot and cold wall temperature (= $(T_H - T_C)$)
$\Delta_{\min, \text{cell}}$	[m]	Minimum cell distance

1. INTRODUCTION

Natural convection of enclosed spaces is widely analysed in heat transfer literature (Refs. [1,2] and references therein) but most of these analyses were carried out for Newtonian fluids in rectangular enclosures. There is limited information in existing literature on natural convection in cylindrical annular enclosures [3-5] in comparison to the vast body of literature on rectangular enclosures. However, the annular cylindrical geometry (i.e. annular space around a cylindrical storage) is more common than rectangular enclosures in engineering applications such as chemical or biological fluid storages, anaerobic digestion tanks, and solar energy collectors. Moreover, the literature on natural convection of inelastic non-Newtonian fluids following power-law viscosity (i.e. $\mu = K\dot{\gamma}^{n-1}$ where μ is the viscosity, K is the consistency, n is the power-law index and $\dot{\gamma}$ is the shear rate) is relatively limited in comparison to the extensive list for Newtonian fluids. Aqueous solutions of polymers including carboxymethyl cellulose, polyethylene oxide, polyacrylamide and xanthan gum exhibit power-law of viscosity. Table 1 of Ref. [6] can be referred for a summary of the outcomes of existing papers on natural convection in enclosures involving power-law fluids. All these analyses reported a strengthening of convection with decreasing n due to the weakening of viscous resistance. Moreover, Yigit *et al.* [6] and references therein deal with rectangular enclosures. Recently, natural convection of power-law fluids in square cross-sectioned vertical annular enclosures with differentially heated vertical walls for both constant wall temperature (CWT) and constant wall heat flux (CWHF) boundary conditions has been analysed [7,8]. Also, the natural convection of power-law fluids in Rayleigh-Bénard configuration in square cross-sectioned cylindrical annular space for active horizontal walls subjected both CWT and CWHF boundary conditions has also recently been analysed by Yigit *et al.* [9] who compared the heat transfer rates for these two boundary conditions and offered physical explanations for the observed differences. It is worth noting that all the analyses on natural convection of power-law fluids deal with annular spaces with square cross-section [7-9].

It has been well-known that the aspect ratio (i.e. height: width) of the enclosure significantly affects the rate of heat transfer in natural convection of Newtonian fluids [10,11]. Moreover, the aspect ratio has been found to have significant influences on the mean Nusselt number for natural convection of power-law fluids

in rectangular enclosures [6,12]. Furthermore, the boundary condition of the active walls does not only affect the numerical value of the mean Nusselt number but also its qualitative variation with aspect ratio for rectangular enclosures with differentially heated vertical sidewalls. For example, the mean Nusselt number shows a non-monotonic aspect ratio dependence for both Newtonian and power-law fluids for CWT boundary condition, whereas the mean Nusselt number increases monotonically with aspect ratio for CWHF boundary condition. Moreover, the mean Nusselt number in square cross-sectional cylindrical annular enclosures with differentially heated sidewalls can be up to 4 times bigger in CWT boundary condition than one in the CWHF configuration for the same set of numerical values of nominal Rayleigh and Prandtl numbers in shear thinning fluids (i.e. $n < 1$) [8]. Thus, it is necessary to analyse the aspect ratio effects on natural convection of power-law fluids in vertical annular enclosures with differentially heated vertical walls for different boundary conditions. The CWT and CWHF boundary conditions are the two most common boundary conditions used in heat transfer literature and heat transfer experiments. The CWT boundary condition can be implemented either by a thermostat or by condensing steam. By contrast, CWHF boundary condition can be obtained by electric coil heating.

The influences of aspect ratio on heat and momentum transport in natural convection of power-law fluids within rectangular cross-sectional annular cylindrical enclosures with differentially heated vertical walls are yet to be investigated in detail. The present analysis focuses on steady-state axisymmetric simulations of natural convection of power-law fluids in cylindrical annular enclosures with a rectangular cross-section for a range of different aspect ratios (i.e. $0.125 \leq AR = H/L \leq 8$, where H is the enclosure height and L is the difference between outer and inner cylinder radius), normalized internal radii $0.125 \leq r_i/L \leq 16$ (where r_i internal cylinder radius), power-law indices (i.e. $0.6 \leq n \leq 1.8$) and nominal Rayleigh numbers (i.e. $Ra = 10^3 - 10^6$) for a single representative nominal value of Prandtl number $Pr = 10^3$. Aqueous solutions of xanthan gum often exhibit Prandtl numbers of the order of 1000. Several previous analyses [6-9,12] revealed that variation of Prandtl number does not have impact on the mean Nusselt number for $Pr > 10^2$ and thus, a single Prandtl number value is considered here. Both CWT and CWHF boundary conditions have been considered for the differentially heated vertical walls in this analysis.

The main objectives of this analysis are:

1. To demonstrate the influences of aspect ratio AR on natural convection of power-law fluids in cylindrical vertical annuli for different values of nominal Rayleigh number and power-law index ranges.
2. To indicate the influences of cylinder radius on natural convection of power-law fluids in vertical cylindrical annuli with differentially heated vertical walls for different values of aspect ratio.
3. To provide physical explanations for the above effects and propose correlations for the mean Nusselt number using computational simulation data.

Mathematical background and numerical implementation related to this analysis will be presented in the next two sections. Following that, a scaling analysis will be provided in order to elucidate the expected influences of $Ra, r_i/L, n$ and AR on the mean Nusselt number. Subsequently, results will be presented along with its discussion. Finally, the conclusions are drawn and main findings are summarised at the last section of this paper.

2. MATHEMATICAL BACKGROUND

According to the power-law model the viscous stress tensor τ_{ij} is expressed as [13]:

$$\tau_{ij} = \mu_a e_{ij} = K(e_{kl}e_{kl}/2)^{(n-1)/2} e_{ij} \quad (1)$$

Here, $e_{ij} = (\partial u_i/\partial x_j + \partial u_j/\partial x_i)$ is the rate of strain tensor, K is the consistency and n is the power-law index and $\mu_a = K(e_{kl}e_{kl}/2)^{(n-1)/2}$ is the apparent viscosity. The apparent viscosity μ_a decreases (increases) with increasing shear rate for $n < 1$ ($n > 1$) and thus fluids with $n < 1$ ($n > 1$) are referred to as shear-thinning (shear-thickening) fluids, whereas $n = 1$ represents Newtonian fluids. According to Buckingham's pi theorem one gets: $Nu = f(Ra, Pr, n, r_i/L, AR)$ where the nominal Rayleigh and Prandtl numbers for power-law fluids can be stated as follows [14-17]:

$$Ra = g\beta\Delta T_{ref}L^{2n+1}/[\alpha^n(K/\rho)]; Pr = (K/\rho)\alpha^{n-2}L^{2-2n} \quad (2)$$

where $g, \beta, \Delta T_{ref}$ are the acceleration due to gravity, volume expansion coefficient and characteristic temperature difference. The characteristic temperature difference ΔT_{ref} can be considered as the difference between hot and cold wall temperatures (i.e. $\Delta T_{ref} = T_H - T_C$) in the CWT boundary

condition, whereas ΔT_{ref} is taken to be $\Delta T_{ref} = q_i L/k$ for CWHF boundary condition. For the current investigation, the Nusselt number for the inner periphery Nu_i is given by:

$$Nu_i = h_i L/k \text{ where } h_i = \left| -k \left(\frac{\partial T}{\partial r} \right)_{r=r_i} \frac{1}{(T_{r=r_i} - T_{r=r_i+L})} \right| \quad (3)$$

with h_i being the local heat transfer coefficient. For steady state heat transfer one gets:

$$\frac{q_i}{q_o} = \frac{r_o}{r_i} = 1 + \frac{L}{r_i} \quad (4)$$

where $q_i = -k \left(\frac{\partial T}{\partial r} \right)_{r=r_i}$ and $q_o = -k \left(\frac{\partial T}{\partial r} \right)_{r=r_o}$ are the heat fluxes in the radial direction on the vertical

walls. The mean Nusselt number based on the inner periphery \overline{Nu}_i can be defined as $\overline{Nu}_i = \overline{h}_i L/k$

where $\overline{h}_i = \frac{1}{H} \int_0^H h_i dx_3$ is the mean heat transfer coefficient at the inner periphery. In this respect, it is

useful to find the mean Nusselt number based on the inner periphery for pure conductive transport,

which can be obtained as a solution of 1D steady heat conduction equation in the radial direction as:

$$Nu_{cond} = \frac{L/r_i}{\ln(1+L/r_i)} \quad (5)$$

Here, a steady-state flow of an incompressible power-law fluid is considered where all the thermophysical properties (e.g. k , c_p , n and K) are taken to be constant. In this analysis, all the governing equations are solved as dimensionless form to generalise the results. The spatial co-ordinates, velocity components, pressure and temperature are expressed in dimensionless form as follows:

$$x_i^+ = x_i/L; u_i^+ = u_i/U_{ref}; P^+ = P/\rho U_{ref}^2; \tau_{ij}^+ = \tau_{ij}L/\rho \alpha U_{ref}; \Theta = (T - T_{ref})/\Delta T_{ref} \quad (6)$$

where $U_{ref} = \alpha/L$ is the reference velocity scale, T_{ref} is the reference temperature. The cold wall

temperature T_C is expressed as reference temperature T_{ref} for CWT boundary condition, whereas the

temperature at the centre of the domain T_{cen} is taken to be the reference temperature for CWHF

boundary condition. The incompressible steady-state mass, momentum and energy equations under the

assumption of axisymmetry can be stated as follows:

Non-dimensional mass conservation equation

$$\frac{1}{r^+} \frac{\partial(r^+ u_r^+)}{\partial r^+} + \frac{\partial u_3^+}{\partial x_3^+} = 0 \quad (7)$$

Non-dimensional momentum conservation equations

Radial direction

$$u_r^+ \frac{\partial u_r^+}{\partial r^+} + u_3^+ \frac{\partial u_r^+}{\partial x_3^+} = -\frac{\partial P^+}{\partial r^+} + \frac{1}{r^+} \frac{\partial(r^+ \tau_{rr}^+)}{\partial r^+} - \frac{\tau_{\phi\phi}^+}{r^+} + \frac{\partial(\tau_{r x_3}^+)}{\partial x_3^+} \quad (8i)$$

Vertical direction

$$u_r^+ \frac{\partial u_3^+}{\partial r^+} + u_3^+ \frac{\partial u_3^+}{\partial x_3^+} = -\frac{\partial P^+}{\partial x_3^+} + RaPr \Theta + \frac{1}{r^+} \frac{\partial(r^+ \tau_{r x_3}^+)}{\partial r^+} + \frac{\partial(\tau_{x_3 x_3}^+)}{\partial x_3^+} \quad (8ii)$$

Non-dimensional energy conservation equation

$$u_r^+ \frac{\partial \Theta}{\partial r^+} + u_3^+ \frac{\partial \Theta}{\partial x_3^+} = \frac{1}{r^+} \frac{\partial}{\partial r^+} \left(r^+ \frac{\partial \Theta}{\partial r^+} \right) + \frac{\partial^2 \Theta}{\partial x_3^+ \partial x_3^+} \quad (9)$$

Here, radial coordinate is r and x_3 axis is taken to align with the vertical direction, whereas the flow is assumed to be independent of the azimuthal direction ϕ . However, $\dot{\gamma}_{\phi\phi}$ takes the form $\dot{\gamma}_{\phi\phi} = u_r/r$ in axisymmetric configuration and thus $\tau_{\phi\phi}$ appears in Eq. (8i). The simulation domain is schematically shown in Fig. 1 which indicates that the two horizontal walls of a rectangular cross-sectional cylindrical enclosure are insulated, whereas the vertical boundaries are taken to be differentially heated. Equations 7-9 are subjected to the following boundary conditions in this configuration:

Velocity boundary conditions

$u_r^+ = 0$ and $u_3^+ = 0$ at $x_3^+ = 0$ and $x_3^+ = AR$ due to no-slip condition and impenetrability on horizontal walls and

$u_r^+ = 0$ and $u_3^+ = 0$ at $r^+ = r_i/L$ and $r^+ = 1 + r_i/L$ due to impenetrability and no-slip condition on vertical walls.

Temperature boundary conditions

$\partial\Theta/\partial x_3^+ = 0$ at $x_3^+ = 0$ and $x_3^+ = AR$ due to adiabatic horizontal walls

$\Theta = 1.0$ at $r^+ = r_i/L$ and $\Theta = 0.0$ at $r^+ = r_i/L + 1$ for the CWT configuration

$-\partial\Theta/\partial r^+ = 1.0$ at $r^+ = r_i/L$ and $-\partial\Theta/\partial r^+ = 1.0/(1 + L/r_i)$ at $r^+ = r_i/L + 1$ for the CWHF configuration.

3. NUMERICAL IMPLEMENTATION

The governing equations (i.e. Eqs. 7-9) are solved iteratively in the context of the finite-volume methodology by applying aforementioned boundary conditions. The convective terms are discretised using a second-order upwind scheme, whereas the diffusive terms are discretised by a second-order

central differencing scheme. The coupling between pressure and velocity is obtained using the well-known SIMPLE (Semi-Implicit Method for Pressure-Linked Equations) algorithm [18]. The criterion of convergence was taken to be 10^{-6} for all the relative (scaled) residuals. The numerical scheme has been validated in the past with respect to the benchmark data of de Vahl Davis [19] for natural convection of Newtonian fluids in square enclosures with differentially heated vertical walls and an excellent agreement was obtained (see Table 3 of Ref. [20]). Moreover, the variation of $\overline{Nu}/\overline{Nu}_{n=1}$ with n for natural convection of power-law fluids in a square enclosure with differentially heated side walls subjected to CWT boundary condition has also been found to be excellent quantitative agreement with the numerical findings of Kim *et al.* [21] (see Fig. 2 of Ref. [22]).

Three different meshes (i.e. M1, M2, and M3) for each AR values have been utilised to ensure grid independence of the results for both Newtonian and power-law fluids. The details of the non-uniform Cartesian meshes, which have been used in current analysis, are listed in Table 1. The maximum numerical uncertainty associated with the mean Nusselt number \overline{Nu}_i based on the inner periphery for both Newtonian (i.e. $n = 1.0$) and power-law fluids has been found to be smaller than 1% between M1, M2 and M3 mesh configurations for the ranges of parameters (i.e. $0.125 \leq r_i/L \leq 16$, $0.6 \leq n \leq 1.8$, $0.125 \leq AR \leq 8$ and $10^3 \leq Ra \leq 10^6$ at $Pr = 10^3$) considered here. The M2 mesh has been used for each AR for the sake of sensitivity of numerical results and optimization of computational economy.

4. SCALING ANALYSIS

A detailed scaling analysis is performed to explain the influences of $Ra, Pr, AR, n, r_i/L$ on the mean Nusselt number \overline{Nu}_i . Equating the order of magnitudes of inertial and buoyancy terms yields $u_3 \sim \sqrt{g\beta(T_H - T_C)LAR}$ ($u_3 \sim \sqrt{g\beta q \delta_{th}LAR/k}$) for CWT (CWHF) configurations. Using continuity equation for axisymmetric geometry, one gets:

$$\frac{1}{r} \frac{\partial(ru_r)}{\partial r} \sim \left(\frac{u_r}{r} + \frac{u_r}{L} \right) \sim \frac{\partial u_3}{\partial x_3} \sim \frac{u_3}{H} \quad (10)$$

which leads to scaling estimate of u_r :

$$u_r \sim \frac{u_3}{AR(1+L/r_i)} \sim \frac{\alpha}{L} \frac{1}{\sqrt{AR}} \frac{\sqrt{Ra_{CWT}Pr}}{(1+L/r_i)}; u_r \sim \frac{u_3}{AR(1+L/r_i)} \sim \frac{\alpha}{L} \frac{Ra_{CWHF}^{(n+1)/(n+4)} Pr^{(n+2)/(n+4)} AR^{-2/(n+4)} f_1^{-3/(n+4)}}{(1+L/r_i)} \quad (11)$$

Similarly, equating the order of magnitudes of inertial and viscous terms in the vertical (radial) direction (i.e. $\rho u_3^2/H \sim [(K/\delta)(u_3/\delta)^n]$ ($\rho u_r^2/L \sim [(K/\delta_1)(u_r/\delta_1)^n]$), it is possible to estimate hydrodynamic boundary layer thickness where $\delta(\delta_1)$ is the hydrodynamic boundary layer thickness on the vertical (horizontal) walls respectively:

$$\delta \sim L Ra_{CWT}^{(n-2)/(2n+2)} Pr^{n/(2n+2)} AR^{n/(2n+2)} \quad (12i)$$

$$\delta \sim L Ra_{CWHF}^{(n-2)/(n+4)} Pr^{n/(n+4)} AR^{n/(n+4)} f_1^{(n-2)/(n+4)} \quad (12ii)$$

$$\delta_1 \sim L Ra_{CWT}^{(n-2)/(2n+2)} Pr^{n/(2n+2)} AR^{(2-n)/(2n+2)} / (1 + L/r_i)^{(n-2)/(n+1)} \quad (13i)$$

$$\delta_1 \sim L Ra_{CWHF}^{(n-2)/(n+4)} Pr^{n/(n+4)} AR^{(4-2n)/[(n+4)(n+1)]} f_1^{(6-3n)/[(n+4)(n+1)]} / (1 + L/r_i)^{(n-2)/(n+1)} \quad (13ii)$$

where the function $f_1(Ra, Pr, AR, n, r_i/L)$ represents the ratio of hydrodynamic and thermal boundary layer thickness (i.e. δ/δ_{th}) on the vertical wall. Using Eqs. 12 and 13, it is possible to estimate the effective viscosity in the vertical (horizontal) boundary layers (i.e. $\mu_{eff}^V \sim K(u_3/\delta)^{n-1}$ ($\mu_{eff}^H \sim K(u_r/\delta_1)^{n-1}$) in order to predict the effective Rayleigh numbers (i.e. $Ra_{eff} = \rho^2 c_p g \beta \Delta T_{ref} L^3 / \mu_{eff} k$) in the vertical and horizontal boundary layers in the following manner:

$$Ra_{CWT,eff}^V = Ra_{CWT}^{(5-n)/(2n+2)} Pr^{(1-n)/(2n+2)} AR^{(1-n)/(2n+2)} \quad (14i)$$

$$Ra_{CWHF,eff}^V = Ra_{CWHF}^{(7-2n)/(n+4)} Pr^{(2-2n)/(n+4)} AR^{(2-2n)/(n+4)} f_1^{-(n+1)(n-1)/(n+4)} \quad (14ii)$$

$$Ra_{CWT,eff}^H = Ra_{CWT}^{(5-n)/(2n+2)} Pr^{(1-n)/(2n+2)} AR^{(3-3n)/(2n+2)} / (1 + L/r_i)^{(3-3n)/(n+1)} \quad (15i)$$

$$Ra_{CWHF,eff}^H = Ra_{CWHF}^{(7-2n)/(n+4)} Pr^{(2-2n)/(n+4)} AR^{(6-6n)/(n+4)} f_1^{(9-9n)/[(n+4)(n+1)]} / (1 + L/r_i)^{(3-3n)/(n+1)} \quad (15ii)$$

Eqs. 14 and 15 shows that the effective value of Rayleigh number attains significantly larger than its nominal value for a decrease in values of n for shear thinning (i.e. $n < 1$) fluids. Furthermore, $Ra_{CWT,eff}^H$ and $Ra_{CWHF,eff}^H$ decrease with decreasing r_i/L for shear thinning (i.e. $n < 1$) fluids. However, $Ra_{CWT,eff}^H$ and $Ra_{CWHF,eff}^H$ increase with decreasing r_i/L for shear thickening (i.e. $n > 1$) fluids.

The mean Nusselt number \overline{Nu}_i can be estimated by using the wall heat flux scaling $q_w \sim k\Delta T/\delta_{th}$ as:

$$\overline{Nu}_{i,CWT} = Ra_{CWT}^{\frac{2-n}{2n+2}} Pr^{-\frac{n}{2n+2}} AR^{-\frac{n}{2n+2}} f_1(Ra_{CWT}, Pr, AR, n, r_i/L) \quad (16i)$$

$$\overline{Nu}_{i,CWHF} = Ra_{CWHF}^{(2-n)/(n+4)} Pr^{-n/(n+4)} AR^{-n/(n+4)} f_1(Ra_{CWHF}, Pr, AR, n, r_i/L)^{(2n+2)/(n+4)} \quad (16ii)$$

Equations 16i and 16ii imply that the exponent of Rayleigh number increases with decreasing n but the exponent remains positive for the range of the values of n considered here. Thus, the mean Nusselt number \overline{Nu}_i is expected to increase with an increase in (a decrease in) nominal Rayleigh number (power-law exponent).

5. RESULTS & DISCUSSION

5.1. Effects of nominal Rayleigh number and power-law index

The distributions of dimensionless temperature $\theta = (T - T_{cen})/\Delta T_{ref}$ and dimensionless axial (radial) $W = u_3L/\alpha$ ($U = u_rL/\alpha$) velocity components along the horizontal (vertical) mid-plane for different Ra and n values at $r_i/L = 1$, $AR = 0.5$ and $Pr = 10^3$ are shown in Fig. 2 for both CWT and CWHF configurations. The distributions of θ for the pure-conduction solution (where fluid flow does not affect thermal transport) are also shown in Fig. 2 by triangles (circles) for CWT (CWHF) configurations. Figure 2 demonstrates that the dimensionless temperature θ distribution between the hot and cold walls of the enclosure deviates significantly from the pure conduction solution with increasing (decreasing) $Ra(n)$, which is indicative of the strengthening of convective thermal transport for both CWT and CWHF configurations. This behaviour can also be seen from the increases in the magnitudes of W and U with increasing (decreasing) $Ra(n)$, as shown in Fig. 2, regardless of the boundary condition. Furthermore, the magnitudes of θ , W and U are found to be smaller in the CWHF configuration than the corresponding values in the CWT configuration, which is an indication of stronger convective thermal transport in the CWT configuration in comparison to that in the CWHF configuration. This can also be confirmed by scaling of wall heat flux on the inner periphery as $q_i \sim k\Delta T/\delta_{th}$ where ΔT and δ_{th} are the characteristic temperature difference and the thickness of thermal boundary layer on vertical walls, respectively. This implies that θ in the case of CWHF boundary condition scales as $\theta \sim \Delta T k/q_i L \sim q_i \delta_{th} k/q_i L k \sim O(\delta_{th}/L)$, whereas $\theta \sim O(1)$ for CWT

boundary condition. Accordingly, the magnitude of θ for the CWHF boundary condition is supposed to decrease with an increase in (a decrease in) $Ra(n)$ because of the thinning of thermal boundary layer thickness. This smaller temperature difference between the vertical walls in the CWHF configuration induces to weaker convection than in the CWT configuration. This is consistent with scaling analysis presented in Eqs. 14 and 15, which indicates that the effective Rayleigh number in the CWHF configuration remains smaller than the corresponding value in the CWT configuration for same set of numerical values of Ra, Pr, n, AR and r_i/L . The contours of dimensionless temperature θ and dimensionless stream function $\Psi = \psi/\alpha$ (where ψ is the dimensional stream function and α is thermal diffusivity) are demonstrated in Fig. 3 for different values of Ra and n for $r_i/L = 1$, $AR = 0.5$ and $Pr = 10^3$ in the case of CWT configuration. Figure 3 shows that the magnitude of Ψ increases and dimensionless temperature contours become increasingly curved with an increase in (a decrease in) $Ra(n)$ due to the strengthening of convective thermal transport. Similar qualitative behaviour has been also observed for CWHF boundary condition but it is not shown here for the sake of conciseness. It is worth noting that these findings are consistent with previous findings [7,8] which dealt with natural convection of power-law fluids in annular spaces with square cross-section (i.e. same configuration for $AR = 1.0$).

5.2. Effects of aspect ratio

The distributions of dimensionless temperature θ and dimensionless axial (radial) W (U) velocity components along the horizontal (vertical) mid-plane for different AR values for $r_i/L = 1$, $Ra = 10^6$, $n = 0.6$ and $Pr = 10^3$ are shown in Fig. 4 for both CWT and CWHF configurations. The dimensionless temperature θ distributions obtained from the pure-conduction solutions (where fluid flow does not affect thermal transport) are also shown in Fig. 4 by the red dashed lines for CWT and CWHF configurations. Figure 4 exhibits that the distribution of θ deviates from the pure conduction solution with increasing AR , which indicates a strengthening of convection with an increase in AR for both CWT and CWHF configurations. Additionally, Fig. 4 indicates that the magnitudes of θ , W and U in the CWHF configuration are smaller than the corresponding values observed for the CWT configuration.

This is also a confirmation of stronger convection in CWT configuration in comparison to that in the CWHF configuration for different AR values with the same set of values of $Ra, Pr, n, r_i/L$. Furthermore, it can be noticed from Fig.4 that the magnitudes of W and U increase with increasing AR for a given set of values of $Ra, Pr, n, r_i/L$ for both CWT and CWHF configurations. This is consistent with the qualitative trends predicted by scaling relations given by Eq. 11. Furthermore, the aspect ratio AR (i.e. AR_{max}) for which the highest \overline{Nu}_i is obtained is indicated by an asterisk in the legend of Fig. 4. This reveals that a non-monotonic AR dependence of the \overline{Nu}_i is obtained in the CWT configuration (e.g. the highest \overline{Nu}_i is obtained at $AR = 0.5$ for $r_i/L = 1, Ra = 10^6, n = 0.6$ and $Pr = 10^3$). By contrast, the highest value of \overline{Nu}_i is obtained for the highest AR case in the CWHF configuration. The variations of \overline{Nu}_i with AR for different values of Ra and n at $r_i/L = 1.0$ and $Pr = 10^3$ are shown in Fig. 5 for both CWT and CWHF configurations. It can clearly be seen from Fig. 5 that the \overline{Nu}_i shows a non-monotonic AR dependence for a given set values of $Ra, Pr, r_i/L$ for shear thinning (i.e. $n < 1$), Newtonian (i.e. $n = 1$) and shear thickening (i.e. $n > 1$) fluids for CWT boundary condition, while a monotonic increase in \overline{Nu}_i was obtained for an increase in values of AR in the CWHF configuration, regardless of the value of n . It can also be noticed from Fig. 5 that AR_{max} is dependent on values of Ra and n for same set of values of r_i/L and Pr in CWT configuration. This is in agreement with previous analyses on the influences of aspect ratio and boundary condition on natural convection in rectangular enclosures for both Newtonian (i.e. $n = 1$) [11] and power-law fluids [12].

The non-monotonic (monotonic) AR dependence of \overline{Nu}_i for CWT (CWHF) boundary condition can be explained in the following manner using the energy flux integral between active walls. The energy flux integral can be shown as follows:

$$\dot{Q} = \dot{Q}_{conv} + \dot{Q}_{cond} = \int_{r_i}^{r_o} \rho c_p T u_3 2\pi r dr - \int_{r_i}^{r_o} k \left(\frac{\partial T}{\partial x_3} \right) 2\pi r dr \quad (17)$$

where the first term on the right-hand side represents the effects of convective transport, whereas the second term on the right-hand side accounts for thermal conduction. Here, \dot{Q}_{conv} and \dot{Q}_{cond} can be scaled in the following manner by using Eqs. 10-13:

$$\dot{Q}_{conv, CWT} \sim \pi (2r_i + L) \rho c_p \Delta T u_3 \delta \sim k \Delta T \pi (2r_i + L) Ra_{CWT}^{(2n-1)/(2n+2)} Pr^{(2n+1)/(2n+2)} AR^{(2n+1)/(2n+2)} \quad (18i)$$

$$\dot{Q}_{conv,CWHF} \sim \pi(2r_i + L) \frac{\rho c_p u_s q_i \delta_{th} \delta}{k} \sim q_i L \pi(2r_i + L) Ra_{CWHF}^{(3n-3)/(n+4)} Pr^{(3n+2)/(n+4)} AR^{(3n+2)/(n+4)} f_1^{(3-3n)/(n+4)} \quad (18ii)$$

$$\dot{Q}_{cond,CWT} \sim k \Delta T \pi(2r_i + L) / AR \quad (19i)$$

$$\dot{Q}_{cond,CWHF} \sim \pi(2r_i + L) \frac{q_i \delta_{th}}{H} \sim q_i L \pi(2r_i + L) Ra_{CWHF}^{(n-2)/(n+4)} Pr^{n/(n+4)} AR^{-4/(n+4)} f_1^{(-2n-2)/(n+4)} \quad (19ii)$$

The scaling estimation in Eqs. 18 and 19 suggest that the influences of convection strengthen with an increase in AR , but the diffusive thermal transport effects weaken with an increase in AR for CWT boundary condition, which is in agreement with previous findings of for power-law and Newtonian fluids [10-12, 23, 24]. The highest value of \overline{Nu}_i is obtained for an optimum value of aspect ratio (i.e. AR_{max}) due to the competition between an enhancement in advection and a weakening of thermal diffusion with an increase in AR . It can be noted from Eq. 18i and 19i that the value of AR_{max} for CWT boundary condition is dependent on Ra for a given set of values of n and Pr , which is consistent with the numerical results presented in Fig. 5. By contrast, the strengthening (weakening) of $\dot{Q}_{conv,CWHF}$ ($\dot{Q}_{cond,CWHF}$) with increasing AR in the CWHF configuration is stronger (weaker) than $\dot{Q}_{conv,CWT}$ ($\dot{Q}_{cond,CWT}$) in the CWT configuration. Thus, \overline{Nu}_i increases monotonically with increasing AR in the CWHF configuration, which is in agreement with previous analyses [11,12] on rectangular enclosures with both Newtonian (i.e. $n = 1$) and power-law fluids.

5.3. Effects of r_i/L

The distributions of dimensionless temperature θ along the horizontal mid-plane for different r_i/L and n values are shown in Fig. 6 at $AR = 0.5$, $Ra = 10^6$ and $Pr = 10^3$ in the case of both CWT and CWHF configurations. Figure 6 indicates that the temperature difference increases with an increase in r_i/L for shear thinning (i.e. $n < 1$), Newtonian (i.e. $n = 1$) and shear thickening (i.e. $n > 1$) fluids in the CWHF configuration. It is important to understand the r_i/L dependence of the temperature difference between vertical walls ΔT due to pure conductive transport in order to explain the wall curvature effects on the temperature difference between vertical walls. It is worth indicating that the temperature difference between vertical walls ΔT is dependent on the internal radius of the cylindrical annular enclosure when the thermal transport occurs purely by conduction. The thermal resistance due to conduction in

axisymmetric cylindrical geometry is given by $\ln(r_o/r_i)/2\pi kL$, which suggests that the steady state heat flow rate for pure conductive transport is given by: $\dot{Q} = \Delta T_{cond}/\{\ln(r_o/r_i)/2\pi kL\}$. Furthermore, \dot{Q} can be expressed in terms of heat flux on the inner periphery as: $\dot{Q} = q_i 2\pi r_i L$, which leads to:

$$\Delta T_{cond} = \frac{q_i L (r_i/L)}{k} \ln\left(1 + \frac{L}{r_i}\right) \quad (20)$$

Eq. (20) indicates that ΔT_{cond} increases with a decrease in values of r_i/L . As the heat transfer coefficient $h_i = q_i/\Delta T$ for convective transport is expected to be greater than that for pure conductive transport $(h_i)_{cond} = q_i/\Delta T_{cond}$, the temperature difference between the vertical walls remains smaller than that in the case of purely conductive transport for the transport regime, where convection plays a significant role in the overall thermal transport. Furthermore, the distributions of dimensionless axial (radial) $W = u_3 L/\alpha$ ($U = u_r L/\alpha$) velocity components along the horizontal (vertical) mid-plane for different r_i/L and n values are shown in Fig.7 at $AR = 0.5$, $Ra = 10^6$ and $Pr = 10^3$ in the case of both CWT and CWHF configurations. It can be seen from Fig. 7 that U increases while W decreases with an increase in r_i/L for shear thinning (i.e. $n < 1$), Newtonian (i.e. $n = 1$) and shear thickening (i.e. $n > 1$) fluids in both CWT and CWHF configurations. This numerical findings can be confirmed by scaling estimation of the radial velocity component given in Eq. 11 (i.e. $u_r \sim u_3(1 + L/r_i)$) for both Newtonian and power-law fluids regardless of the boundary condition. As the variations W and U with r_i/L exhibit opposite behaviours, as shown in the Fig.7, the relative contributions of thermal transport due to convection and conduction for different values of r_i/L can be explained from the variations of $\overline{Nu}_i/Nu_{cond}$ with r_i/L . It is worth noting that Nu_{cond} increases with a decrease in r_i/L (see Eq. 5). Therefore, the variations of $\overline{Nu}_i/Nu_{cond}$ with r_i/L for different values of n and AR at $Ra = 10^6$ and $Pr = 10^3$ are shown in Fig. 8 for both CWT and CWHF configurations. Figure 8 exhibits that $\overline{Nu}_i/Nu_{cond}$ increases with an increase in r_i/L and approaches asymptotically to the value of the mean Nusselt number \overline{Nu}_{Rec} for the corresponding rectangular enclosures (i.e. in the limit of $r_i/L \rightarrow \infty$). This suggests that the relative contribution of convection to overall thermal transport increases with an increase in r_i/L . This is in a full agreement with previous results for Newtonian fluids [3-5] and for power-law fluids [7,8].

This behaviour of $\overline{Nu}_i/Nu_{cond}$ with increasing r_i/L agrees with scaling relations presented in Eq. 14 and 15, which indicates Ra^H_{eff} remains smaller than Ra^V_{eff} in cylindrical annular enclosures, regardless of the boundary condition. The above findings indicate that relative influence of convection on the overall thermal transport is weaker in cylindrical annular enclosures than in rectangular enclosures and the relative strength of convection augments with an increase in internal cylinder radius.

5.4. Correlations for mean Nusselt number

Turan *et al.* [12] proposed a correlation for the mean Nusselt number for natural convection of power-law fluids in rectangular enclosures (i.e. \overline{Nu}_{Rec}) with differentially heated vertical walls for CWT configuration for the range of nominal Rayleigh number $10^4 \leq Ra_{CWT} \leq 10^6$:

For $Ra_{CWT}AR^7 \geq 10^4$:

$$\overline{Nu}_{Rec} = \text{Max} \left\{ 1.0, 0.162 \frac{Ra_{CWT}^{0.043} Pr^{0.341}}{(1+Pr)^{0.091}} \left[\frac{Ra_{CWT}^{2-n}}{(Pr^n AR^n)} \right]^{\frac{1}{2(n+1)}} e^{b_{CWT}(n-1)} \times [e^{1-AR^{-0.212}}] \right\} \quad (21i)$$

For $Ra_{CWT}AR^7 < 10^4$ and $Ra_{CWT}AR^5/n^9 \geq 40$:

$$\overline{Nu}_{Rec} = \text{Max} \left\{ 1.0, 0.162 \frac{Ra_{CWT}^{0.043} Pr^{0.341}}{(1+Pr)^{0.091}} \left[\frac{Ra_{CWT}^{2-n}}{(Pr^n AR^n)} \right]^{\frac{1}{2(n+1)}} e^{b_{CWT}(n-1)} \times [1 - 1.5(1 - AR)^{b_2}] \right\} \quad (21ii)$$

where $b_{CWT} = 1.343Ra_{CWT}^{0.065} Pr^{0.036} AR^{0.099}$ ($b_{CWT} = 0.858Ra_{CWT}^{0.071} Pr^{0.034} AR^{-0.006}$) for $n \leq 1$ ($n > 1$) and

$b_2 = 0.156Ra_{CWT}^{0.222} n^{-0.887}$ ($b_2 = 0.725Ra_{CWT}^{0.104} n^{-1.030}$) for $n \leq 1$ ($n > 1$)

For $Ra_{CWT}AR^7 < 10^4$ and $Ra_{CWT}AR^5/n^9 < 40$:

$$\overline{Nu}_{Rec} = 1 + \left(\frac{1}{4.95} \right)^{4+4/n} Ra_{CWT}^{2/n} AR^{4+4/n} \quad (21iii)$$

Similarly, Turan *et al.* [12] proposed the following correlation for the mean Nusselt number \overline{Nu}_{Rec} for natural convection of power-law fluids in rectangular enclosures with differentially heated vertical walls for CWHF configuration for the range of nominal Rayleigh number $10^4 \leq Ra_{CWHF} \leq 10^6$:

For $AR \geq 1$:

$$\overline{Nu}_{Rec} = \text{Max} \left\{ 1.0, \frac{0.209Ra_{CWHF}^{0.049} Pr^{0.231}}{(1+Pr)^{0.031}} \left[\frac{Ra_{CWHF}^{1-n/2}}{(Pr^{n/2} AR^{n/2})} \right]^{\frac{1}{n/2+2}} e^{b_{CWHF}(n-1)} \times [c_3 \ln(AR) + 1] \right\} \quad (22i)$$

For $AR < 1$ and $Ra_{CWHF}AR^5/n^9 \geq 150$:

$$\overline{Nu}_{Rec} = Max \left\{ 1.0, \frac{0.209 Ra_{CWHF}^{0.049} Pr^{0.231}}{(1+Pr)^{0.031}} \left[\frac{Ra_{CWHF}^{1-n/2}}{(Pr^{n/2} AR^{n/2})} \right]^{\frac{1}{\frac{n}{2}+2}} e^{b_{CWHF}(n-1)} \times [1 - 1.168(1 - AR)^{c_2}] \right\} \quad (22ii)$$

For $AR < 1$ and $Ra_{CWHF} AR^5 / n^9 < 150$:

$$\overline{Nu}_{Rec} = 1 + \left(\frac{1}{4.95} \right)^{4+4/n} Ra_{CWHF}^{2/n} AR^{4+4/n} \quad (22iii)$$

where;

$$b_{CWHF} = 0.965 Ra_{CWHF}^{0.038} Pr^{0.072} AR^{0.034} \quad (b_{CWHF} = 0.815 Ra_{CWHF}^{0.052} Pr^{0.063} AR^{0.046} \text{ for } n \leq 1 \text{ (} n > 1 \text{)}) \quad (22iv)$$

$$c_2 = 0.382 Ra_{CWHF}^{0.121} n^{-0.586} \quad (c_2 = 0.683 Ra_{CWHF}^{0.069} n^{-0.186}) \text{ for } n \leq 1 \text{ (} n > 1 \text{)} \quad (22v)$$

$$c_3 = 0.737 Ra_{CWHF}^{-0.061} n^{0.347} \quad (c_3 = 0.737 Ra_{CWHF}^{-0.061} n^{0.595}) \text{ for } n \leq 1 \text{ (} n > 1 \text{)} \quad (22vi)$$

It is worth noting the correlation given by Eqs. 21 and 22 can be utilised for $r_i/L \gg 1$ where Nu_{cond} approaches unity in the limit of $r_i/L \rightarrow \infty$. Based on numerical findings, the mean Nusselt number \overline{Nu}_i is parametrised here as follows:

$$\overline{Nu}_i = \overline{Nu}_{Rec} \frac{[m(L/r_i)]^d}{\ln\{1+[m(L/r_i)]^d\}} \quad (23)$$

For CWT boundary condition;

For $AR < 1, n \leq 1$;

$$m = 0.975^{(\overline{Nu}_{Rec}-1)}, d = \left\{ (1.471 - 0.075 \ln \left(\frac{Ra_{CWT} AR^5}{n^9} \right)) \right\}^{(\overline{Nu}_{Rec}-1)} \text{ for } \frac{Ra_{CWT} AR^5}{n^9} \leq 3125 \quad (24i)$$

$$m = 0.975^{(\overline{Nu}_{Rec}-1)}, d = \left\{ (0.955 + 0.002 \ln \left(\frac{Ra_{CWT} AR^5}{n^9} \right)) \right\}^{(\overline{Nu}_{Rec}-1)} \text{ for } \frac{Ra_{CWT} AR^5}{n^9} > 3125 \quad (24ii)$$

For $AR \geq 1, n \leq 1$;

$$m = \{(1.218 - 0.506n) + 0.016n^{2.52} \ln Ra_{CWT}\}^{(\overline{Nu}_{Rec}-1)} \quad (24iii)$$

$$d = \left\{ \left(\frac{0.592 - 1.385n}{1 - 2.208n} \right) + \left(\frac{1 - 2.274n}{37.5 - 95.43n} \right) \ln Ra_{CWT} \right\}^{(\overline{Nu}_{Rec}-1)} \quad (24iv)$$

For $n > 1$;

$$m = d = (0.9)^{(\overline{Nu}_{Rec}-1)} \quad (24v)$$

Similarly for CWHF boundary condition;

For $AR < 1, n \leq 1$;

$$m = 0.85^{(\overline{Nu}_{Rec}-1)}, d = \left\{ (0.746 - 0.039 \ln \left(\frac{Ra_{CWHF} AR^5}{n^9} \right)) \right\}^{(\overline{Nu}_{Rec}-1)} \text{ for } \frac{Ra_{CWHF} AR^5}{n^9} \leq 970 \quad (25i)$$

$$m = 0.85^{(\overline{Nu}_{Rec}-1)}, d = \left\{ (0.309 + 0.042 \ln \left(\frac{Ra_{CWHF} AR^5}{n^9} \right)) \right\}^{(\overline{Nu}_{Rec}-1)} \text{ for } \frac{Ra_{CWHF} AR^5}{n^9} > 970 \quad (25ii)$$

For $AR \geq 1, n \leq 1$;

$$m = \left\{ (0.208 - 0.057 n^{4.19}) \ln Ra_{CWHF} \left(\frac{1-0.932n}{1.763-1.66n} \right) \right\}^{(\overline{Nu}_{Rec}-1)} \quad (25iii)$$

$$d = \left\{ (0.794 - 0.1 n^{3.84}) + \left(\frac{1-0.605n}{85.83-61.63n} \right) \ln Ra_{CWHF} \right\}^{(\overline{Nu}_{Rec}-1)} \quad (25iv)$$

For $n > 1$;

$$m = d = (0.7 + 0.01 \ln Ra_{CWHF})^{(\overline{Nu}_{Rec}-1)} \quad (25v)$$

According to Eq. 23, \overline{Nu}_i becomes equal to \overline{Nu}_{Rec} in the limit of $r_i/L \rightarrow \infty$. Furthermore, m and d assume the values of unity when $\overline{Nu}_{Rec} = 1.0$ which indicates that heat transfer occurs purely due to conduction. Accordingly, the unity value of \overline{Nu}_{Rec} also ensures $\overline{Nu}_i = Nu_{cond} = (L/r_i)/(1 + \ln(L/r_i))$, which is the value of the mean Nusselt number for pure conduction in cylindrical annular enclosures with differentially heated vertical walls. The correlation of \overline{Nu}_i given by Eq. 23 has been obtained using a non-linear regression method [25]. The predictions of Eq. 23 are shown in Fig. 9, which demonstrates that the correlation satisfactorily ($R^2 > 0.98$ and 3% maximum error percentage apart from over-prediction in the case of $AR = 0.25$ for shear thinning fluids) predicts \overline{Nu}_i for $0.6 \leq n \leq 1.8, 10^3 \leq Ra \leq 10^6, 0.125 \leq AR \leq 8, 0.125 \leq r_i/L \leq 16$ for both CWT and CWHF boundary conditions.

6. CONCLUSIONS

The effects of aspect ratio on natural convection of power-law fluids in rectangular cross-sectional cylindrical annular enclosures with differentially heated vertical side walls have been numerically investigated in this analysis for both CWT and CWHF boundary conditions for active walls. The influence of thermal convection has been found to be stronger (weaker) in shear thinning (i.e. $n < 1$) (shear thickening (i.e. $n > 1$)) fluids than Newtonian fluids for the same set of values of $Ra, Pr, AR, r_i/L$ regardless of the boundary condition. This is reflected in an increase in the mean Nusselt number \overline{Nu}_i with

a decrease in power-law exponent. The mean Nusselt number \overline{Nu}_i in the CWT boundary condition has been shown to follow a non-monotonic AR dependence for shear thinning (i.e. $n < 1$), Newtonian (i.e. $n = 1$) and shear thickening (i.e. $n > 1$) fluids, whereas \overline{Nu}_i increases monotonically with increasing AR in the case of CWHF configuration irrespective of the value of n . This non-monotonic AR dependence of the mean Nusselt number \overline{Nu}_i originates as a result the competition between the strengthening of convective thermal transport and the weakening of thermal diffusion with increasing aspect ratio AR . The aspect ratio AR_{max} , at which the mean Nusselt number \overline{Nu}_i attains its peak value in the CWT configuration, depends on the nominal value of Rayleigh number for shear thinning (i.e. $n < 1$), Newtonian (i.e. $n = 1$) and shear thickening (i.e. $n > 1$) fluids. The strengthening of thermal convection with increasing AR is much stronger than the weakening of thermal diffusion in the case of CWHF boundary condition which gives rise to a monotonic increase of \overline{Nu}_i with an increase in AR . Moreover, the mean Nusselt number \overline{Nu}_i decreases with increasing r_i/L before approaching the corresponding mean Nusselt number value for a rectangular enclosure in the limit of $r_i/L \rightarrow \infty$. By contrast \overline{Nu}_i normalised by the corresponding Nusselt number for pure conduction (i.e. $\overline{Nu}_i/Nu_{cond}$) increases with increasing r_i/L because Nu_{cond} decreases with increasing r_i/L for cylindrical annular enclosures (i.e. $Nu_{cond} = (L/r_i)/(\ln(1 + L/r_i))$). An increase in $\overline{Nu}_i/Nu_{cond}$ with increasing r_i/L is a reflection of the augmentation of the ratio of convective to conductive transport. A detailed scaling analysis has been utilised to explain the influences of normalised radius, aspect ratio, nominal Rayleigh and Prandtl numbers and power-law index on \overline{Nu}_i for natural convection of power-law fluids within rectangular cross-sectional cylindrical annular enclosures with different values of aspect ratio. Finally, new correlations have been proposed for \overline{Nu}_i for both CWT and CWHF boundary conditions, which have been demonstrated to provide satisfactorily predictions of \overline{Nu}_i for the range of the parameters considered in this analysis. The outcomes of present analysis (i.e. scaling relations, \overline{Nu}_i correlation) will be not only be useful for future experiments on this topic but also for designing and improving thermal systems in many important industrial applications (i.e. food and chemical processing, solar collectors, cooling of electronic equipment).

REFERENCES

- [1] S. Ostrach, Natural convection in enclosure, *J. Heat Trans.*, 110 (1988), 1175-1190.
- [2] E. Bodenschatz, W. Pesch, G. Ahlers, Recent Developments in Rayleigh-Bénard convection, *Ann. Rev. Fluid Mech.*, 32 (2000), 709-778.
- [3] G. de Vahl Davis and R. W. Thomas, Natural convection between concentric vertical cylinder, *Physics of Fluids*, 12 (1969), 198-207.
- [4] B.V.K Satya Sai, K.N. Seetharamu, P.A. Aswatha Narayana and J.N. Reddy, Finite element analysis of the effect of radius ratio on natural convection in an annular cavity, *Int. J. of Numerical Methods for Heat & Fluid Flow*, 3 (1993) 305-318.
- [5] M. Keyhani, F. A. Kulacki and R. N. Christensen, Free convection in a vertical annulus with constant heat flux at the inner wall, *J. Heat Transfer Transactions of ASME*, 105 (1983), 454-459.
- [6] S. Yigit, R.J. Poole, N. Chakraborty, Aspect ratio effects on laminar Rayleigh-Bénard convection of power-law fluids in rectangular enclosures: A numerical investigation, *Int. J. Heat and Mass Trans.*, 91 (2015), 1292-1307.
- [7] S. Yigit, T. Graham, R.J. Poole, N. Chakraborty, Numerical investigation of steady-state laminar convection of power-law fluids in square cross-sectioned cylindrical annular cavity with differentially-heated vertical walls, *Int. J. of Numerical Methods for Heat & Fluid Flow*, 26 (2015), 85-107.
- [8] S. Yigit, J. Ford, R.J. Poole, N. Chakraborty, Numerical investigation of boundary condition effect on laminar natural convection of power-law fluids in square cross-sectional cylindrical annular space with differentially heated vertical walls, *Comput. Therm. Sci.*, 7 (2015), 261-282.
- [9] S. Yigit, C. McRoberts, N. Chakraborty, Numerical investigation of laminar Rayleigh-Bénard convection of power-law fluids in square cross-sectional cylindrical annular enclosures, *Int. Com. in Heat and Mass Transfer*, 78 (2016), 112-120.
- [10] A.A. Ganguli, A. B. Pandit, J.B. Joshi, CFD simulation of heat transfer in a two-dimensional vertical enclosure, *Chem. Eng. Research and Design*, 877 (2009), 711-727.

- [11] O. Turan, R.J. Poole, N. Chakraborty, Influences of boundary conditions on laminar natural convection in rectangular enclosures with differentially heated side walls, *Int. J. Heat and Fluid Flow*, 33 (2012), 131-146.
- [12] O. Turan, A. Sachdeva, R.J. Poole, N. Chakraborty, Aspect ratio and boundary conditions on laminar natural convection of power-law fluids in rectangular enclosures with differentially heated vertical sidewalls, *Int. J. Heat and Mass Trans.*, 60 (2013), 625-639.
- [13] H. Ozoe, S. W. Churchill, Hydrodynamic stability and natural convection in Ostwald-De Waele and Ellis fluids: the development of a numerical solution, *AIChE J.*, 18(1972), 1196-1207.
- [14] M. Lamsaadi, M. Naïmi, M. Hasnaoui, Natural convection of non-Newtonian power law fluids in a shallow horizontal rectangular cavity uniformly heated from below, *Heat Mass Transfer*, 41 (2005) 239-249.
- [15] M. Lamsaadi, M. Naïmi, M. Hasnaoui, Natural convection heat transfer in shallow horizontal rectangular enclosures uniformly heated from the side and filled with non-Newtonian power law fluids, *Energy Conversion and Management*, 47 (2006), 2535 -2551.
- [16] O. Turan, J. Lai, R.J. Poole, N. Chakraborty, Laminar natural convection of power-law fluids in a square enclosure submitted from below to a uniform heat flux density, *J. Non-Newt. Fluid Mech.*, 199 (2013), 80-95.
- [17] O. Turan, F. Fotso-Choupe, J. Lai, R.J. Poole and N. Chakraborty, Boundary condition effects on laminar natural convection of power-law fluids in a square enclosure heated from below with differentially heated horizontal walls, *Ind. Eng. Chem. Res*, 53 (2014), 456-473.
- [18] S. V. Patankar, *Numerical Heat Transfer and Fluid Flow*, Hemisphere, Washington D.C, 1980.
- [19] G. de Vahl Davis, Natural convection of air in a square cavity: A bench mark numerical solution, *Int. J. Numer. Meth. Fluids*, 3 (1983), 249–264.
- [20] O. Turan O, N. Chakraborty, R. J. Poole, Laminar natural convection of Bingham fluids in a square enclosure with differentially heated side walls, *J. non-Newt. Fluid Mech.*, 165 (2010), 901-913.
- [21] G.B. Kim, J.M. Hyun, H.S. Kwak, Transient buoyant convection of a power law non-Newtonian fluid in an enclosure, *Int. J. Heat Mass Transfer*, 46 (2003), 3605-3617.

- [22] O. Turan, A. Sachdeva, N. Chakraborty, R.J. Poole, Laminar natural convection of power-law fluids in a square enclosure with differentially heated side walls subjected to constant wall temperatures, *J. Non-Newt. Fluid Mech.*, 166 (2011), 1049-1063.
- [23] A. Bejan, C. L. Tien, Laminar natural convection heat transfer in a horizontal cavity with different end temperatures, *J. Heat Transfer*, 100 (1978), 641-647.
- [24] A. Bejan, A synthesis of analytical results for natural convection heat transfer across rectangular enclosures, *Int. J. Heat and Mass Transfer*, 23 (1980), 723-726.
- [25] M.A. Brown, A step by step guide to non-linear regression analysis of experimental data using a Microsoft Excel spreadsheet, *Comp. Methods and Programs in Biomedicine*, 65 (2001), 191-200.

Table 1: Summary of the non-uniform Cartesian meshes have been used in current analysis for $0.125 \leq r_i/L \leq 16$, $0.6 \leq n \leq 1.8$, $0.125 \leq AR \leq 8$ and $10^3 \leq Ra \leq 10^6$ at $Pr = 10^3$ with dimensionless minimum cell distance ($\Delta_{min,cell}/L$) and grid expansion ratio (r_e) values.

AR = 0.125			
Grid	M1 (120 × 180)	M2 (160 × 200)	M3 (200 × 220)
$\Delta_{min,cell}/L$	4.176×10^{-4}	3.135×10^{-4}	2.509×10^{-4}
r_e	1.013	1.01	1.008
AR = 0.25			
Grid	M1 (160 × 180)	M2 (180 × 220)	M3 (200 × 240)
$\Delta_{min,cell}/L$	6.270×10^{-4}	5.575×10^{-4}	5.018×10^{-4}
r_e	1.01	1.009	1.008
AR = 0.5			
Grid	M1 (180 × 220)	M2 (200 × 240)	M3 (220 × 260)
$\Delta_{min,cell}/L$	1.115×10^{-3}	1.003×10^{-3}	9.127×10^{-4}
r_e	1.009	1.008	1.007
AR = 1.0			
Grid	M1 (180 × 180)	M2 (240 × 240)	M3 (260 × 260)
$\Delta_{min,cell}/L$	2.230×10^{-3}	1.673×10^{-3}	1.545×10^{-3}
r_e	1.009	1.006	1.006
AR = 2.0			
Grid	M1 (140 × 300)	M2 (160 × 320)	M3 (200 × 400)
$\Delta_{min,cell}/L$	2.678×10^{-3}	2.508×10^{-3}	2.007×10^{-3}
r_e	1.01	1.01	1.008
AR = 4.0			
Grid	M1 (140 × 400)	M2 (160 × 480)	M3 (200 × 600)
$\Delta_{min,cell}/L$	2.865×10^{-3}	2.508×10^{-3}	2.007×10^{-3}
r_e	1.01	1.01	1.008
AR = 8.0			
Grid	M1 (140 × 480)	M2 (160 × 540)	M3 (180 × 560)
$\Delta_{min,cell}/L$	2.865×10^{-3}	2.508×10^{-3}	2.230×10^{-3}
r_e	1.01	1.009	1.009

FIGURE CAPTIONS

Fig. 1: Schematic diagram of the simulation domain: a) CWT, b) CWHF configurations.

Fig. 2: Variations of dimensionless temperature θ and dimensionless axial (radial) $W = u_3L/\alpha$ ($U = u_rL/\alpha$) velocity components along the horizontal (vertical) mid-plane for different Ra and n values at $r_i/L = 1$, $AR = 0.5$ and $Pr = 10^3$. The pure conduction solution is shown by the triangle (circle) for the CWT (CWHF) configuration.

Fig. 3: Contours of the dimensionless isotherms (θ) and dimensionless stream functions (Ψ) for different values of Ra and n at $r_i/L = 1$, $AR = 0.5$ and $Pr = 10^3$ for the CWT configuration.

Fig. 4: Variations of dimensionless temperature θ and dimensionless axial (radial) $W = u_3L/\alpha$ ($U = u_rL/\alpha$) velocity components along the horizontal (vertical) mid-plane for different AR values at $r_i/L = 1$, $Ra = 10^6$, $n = 0.6$ and $Pr = 10^3$ for both CWT and CWHF configurations. The pure conduction solution is shown by the dashed line. The AR values indicated by an asterisk in the legend represent highest \overline{Nu}_i is obtained as shown in Fig. 5.

Fig. 5: Variations of \overline{Nu}_i with AR for different values of Ra and n at $r_i/L = 1.0$ and $Pr = 10^3$.

Fig. 6: Variations of dimensionless temperature θ along the horizontal mid-plane for different r_i/L and n values at $AR = 0.5$, $Ra = 10^6$, $Pr = 10^3$ for both CWT and CWHF configurations. The pure conduction solution is shown by the dashed line.

Fig. 7: Variations of dimensionless axial (radial) W (U) velocity components along the horizontal (vertical) mid-plane for different r_i/L and n values at $AR = 0.5$, $Ra = 10^6$ and $Pr = 10^3$ for both CWT and CWHF configurations.

Fig. 8: Variations of $\overline{Nu}_i/Nu_{cond}$ with r_i/L for different values of n and AR at $Ra = 10^6$ and $Pr = 10^3$ for both CWT and CWHF configurations. The dashed lines represent corresponding value of mean Nusselt number for rectangular enclosures for each AR values.

Fig. 9: Variations of \overline{Nu}_i with r_i/L for different values of n and AR at $Ra = 10^5$ and $Pr = 10^3$ along with predictions of Eq. 23 for both CWT and CWHF configurations. The dashed lines represent Eq. 21 and 22, which are corresponding value of the mean Nusselt number for rectangular enclosures for CWT and CWHF configurations respectively.